Available online at www.sciencedirect.com
ScienceDirect
Surface & Coatings Technology 202 (2008) 3787–3796
SURFACE & COATINGS TECHNOLOGY
www.elsevier.com/locate/surfcoat

Pre-oxidation and TGO growth behaviour of an air-plasma-sprayed thermal barrier coating

W.R. Chen [a,*], X. Wu [a], B.R. Marple [b], R.S. Lima [b], P.C. Patnaik [a]

[a] Institute for Aerospace Research, SMPL, National Research Council Canada, Ottawa, Ontario, Canada K1A 0R6
[b] Industrial Materials Institute, National Research Council Canada, Boucherville, Québec, Canada J4B 6Y4

Received 28 September 2007; accepted in revised form 20 January 2008
Available online 2 February 2008

Abstract

In thermal barrier coating (TBC) systems, spinel and nickel oxide formed in an oxidizing environment are believed to be detrimental to TBC durability during service at high temperatures. The present study shows that in an air-plasma-sprayed (APS) TBC with Co–32Ni–21Cr–8Al–0.5Y (wt.%) bond coat, pre-oxidation treatments in low-pressure oxygen environments can suppress the formation of the detrimental oxides by promoting the formation of an Al_2O_3 layer at the ceramic topcoat/bond coat interface. The development of the thermally grown oxide (TGO) layer generally exhibits a three-stage growth phenomenon that resembles high temperature creep. The pre-oxidation treatments reduce the growth rate and extend the steady-state growth stage, leading to an improved durability. Crack propagation in the TBC proceeds via opening and growth of pre-existing discontinuities in the ceramic topcoat, assisted by crack nucleation and growth associated with the TGO. Crack propagation during thermal cycling appeared to be controlled by TGO growth, and the maximum crack length and TGO thickness generally have a power law relationship.

Keywords: TBC; CoNiCrAlY; Pre-oxidation; Thermal cycling; TGO growth; Crack propagation

1. Introduction

The metallic bond coat (BC), usually MCrAlY, where M = Ni and/or Co, is an important constituent of thermally sprayed TBC systems. It enhances the adhesion of the ceramic thermal barrier layer (the topcoat or TC) to the substrate and also provides oxidation and corrosion protection to the substrate metal. At elevated temperatures, however, oxidation of the bond coat results in the formation of a TGO layer at the ceramic/bond coat interface. If the TGO were composed of a continuous scale of Al_2O_3, it would act as a diffusion barrier to suppress the formation of other detrimental oxides during an extended thermal exposure in service, thus helping to protect the substrate from further oxidation and improving the durability of the system under service conditions. However, it has been reported that some other oxides such as chromia $(Cr,Al)_2O_3$, spinel $Ni(Cr,Al)_2O_4$ and nickel oxide NiO [1–6], may form along with this TGO layer in APS-produced TBC systems. Since oxidation of the bond coat has been recognized as the cause for separation of the ceramic layer from the substrate [2,3,7], the formation of the detrimental oxides will promote crack nucleation during thermal exposure, leading to premature TBC failure [6]. Studies also showed that a continuous Al_2O_3 layer could develop at the ceramic/bond coat interface in thermally sprayed TBC systems via a heat treatment in low oxygen pressure conditions [6,8,9] and therefore, properly pre-oxidizing the TBCs in such conditions may improve TBC durability.

In past studies, the coating oxidation kinetics was usually quantified by measuring the specific weight change during thermal exposure at elevated temperatures [10–14]. The results generally showed a parabolic weight-gain behaviour at first, followed by weight losses. The weight loss was due to scaling off of the oxide scale formed on the surface of the coating, and therefore the weight-gain method may not be suitable to characterize the entire oxidation process. The parabolic growth behaviour was also

* Corresponding author. IAR-SMPL, NRC Canada, 1200 Montreal Road, Building M-17, Ottawa, Ontario, Canada K1A 0R6. Tel.: +1 613 993 4321; fax: +1 613 990 7444.
E-mail address: weijie.chen@nrc-cnrc.gc.ca (W.R. Chen).

0257-8972/$ - see front matter.
doi:10.1016/j.surfcoat.2008.01.021

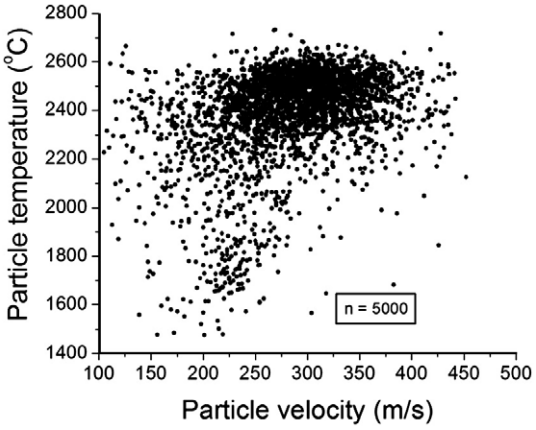

Fig. 1. Distribution of temperature and velocity of CoNiCrAlY particles in the air plasma spray jet.

observed by measuring the thickness of the oxide layer [15–17]; however, more extensive characterization still needs to be done.

In the present investigation, heat treatments in environments with low oxygen pressure were performed to produce an Al_2O_3 layer at the interface between the ceramic topcoat and the bond coat, prior to prolonged thermal exposure in air. The influence of the pre-oxidation treatments on oxidation behaviour was then studied in terms of TGO growth, crack nucleation and propagation, as well as durability of the APS-TBC system.

2. Experimental

The TBC samples consisted of a CoNiCrAlY bond coat and a ZrO_2–8 wt.%Y_2O_3 topcoat. The bond coat was deposited to a thickness of 140–180 μm by the air plasma spray (APS) technique (F4-MB, Sulzer Metco, Westbury, NY, USA), with powders of Co–32Ni–21Cr–8Al–0.5Y (wt.%) (Amdry 9951, Sulzer Metco, Westbury, NY, USA), onto ϕ16 mm × 10 mm Inconel 625 disks. On top of the CoNiCrAlY, the topcoat was deposited to a thickness of 250–280 μm also by the APS technique, employing the same plasma spray torch, with powders of ZrO_2–8 wt.%Y_2O_3 (Metco 204NS, Sulzer Metco, Westbury, NY, USA). The nominal particle size distributions for the BC and TC powders were 5–37 μm and 11–125 μm, respectively. The BC and TC were produced based on the spray parameters recommended by the manufacturer of the torch and feedstock (Sulzer Metco).

For the CoNiCrAlY powder, the particle and velocity values in the plasma jet were monitored using a diagnostic tool based on pyrometric and time-of-flight measurements (DPV 2000, Tecnar Automation, Saint Bruno, QC, Canada). A total of 5000 particles were measured at the centerline of the spray jet where the particle flow density was the highest. The particle temperature and velocity were determined at a distance at which the substrate would normally be positioned when depositing a coating, i.e., 145 mm.

Some of the as-sprayed samples were heat-treated in a vacuum furnace at $<10^{-5}$ Torr ($P_{O2}<2.8\times10^{-4}$ Pa) and 1080 °C for 4 h (vacuum heat treatment or VHT), and some others were heat-treated in a low-pressure oxygen environment of about 2×10^{-3} Torr ($P_{O_2}\approx0.056$ Pa) at 1080 °C for 24 h (low-pressure oxidation treatment or LPOT). The as-sprayed, VHT and LPOT samples were subsequently subjected to thermal cycling in air. The thermal cycle consisted of 8–12-min ramping, 45-min holding at 1050 °C, and 30–40-min cooling to the ambient temperature (25 °C). The oxidized samples were sectioned after completion of a predetermined number of thermal cycles between 1 and 2100, mounted using epoxy, and mechanically polished. The specimens were then examined using a Philips XL30S FEG scanning electron microscope (SEM) with an energy-dispersive spectrometer (EDS). The area and length of TGO, as well as the crack length in the TBC, were measured using ImageTool

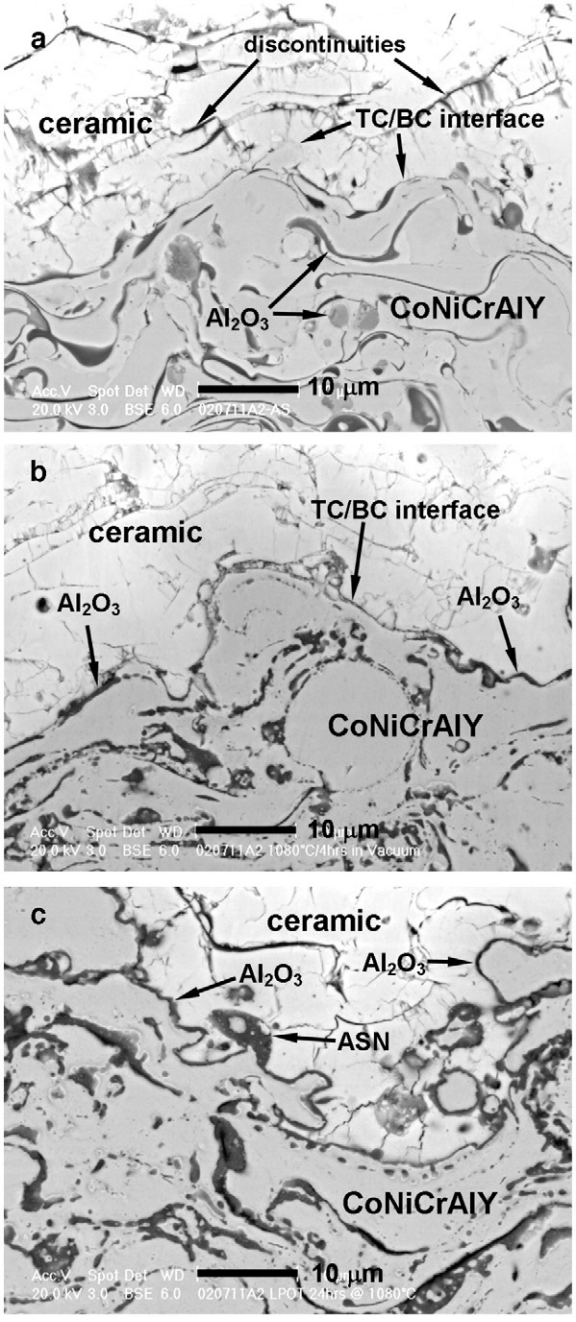

Fig. 2. Microstructures of (a) as-sprayed, (b) VHT and (c) LPOT TBCs with APS-CoNiCrAlY bond coat.

Table 1
Aluminum concentration in the APS-CoNiCrAlY bond coat

	at.% Al
As-sprayed	9.6–17.9
VHT	8.2–10.7
LPOT	8.3–10.5

software, based on the micrographs taken from the cross sections of the tested samples. More than 50 micrographs were taken from each sample for the TGO measurement.

3. Results

3.1. In-flight BC particle characteristics and as-sprayed and pre-oxidized coating microstructures

The average CoNiCrAlY particle temperature and velocity during air plasma spraying were 2388±209 °C and 282±58 m/s, respectively. It was observed that the distributions of particle temperature and velocity in the plasma jet were highly non-uniform (Fig. 1), despite the narrow particle size distribution of the feedstock (5–37 μm). The as-sprayed bond coat contained segmented Al_2O_3 veins (Fig. 2a) within the bond coat but also at the interface between the ceramic topcoat and the bond coat, as a result of partial oxidation of the bond coat during coating deposition. Also, the composition and microstructure of the as-sprayed bond coat were not uniform, containing some non-molten and/or resolidified particles that were entrapped in the coating, due to the wide distributions of particle temperature and velocity during plasma spraying (Fig. 1). SEM/EDS semi-quantitive analysis showed that the aluminum concentration was highly non-uniform in the as-sprayed bond coat, with some regions having very low Al content (Table 1), compared to that in the CoNiCrAlY powder (≈16 at.%). This non-uniformity of Al distribution in the bond coat can probably be attributed to the preferential oxidation and/or vaporization in the plasma, because the particle surface temperature was much higher than the melting point of the CoNiCrAlY (~1300 °C). The ceramic coat, on the other hand, contained porosity and some crack-like discontinuities, having a maximum dimension in the range of 70–100 μm.

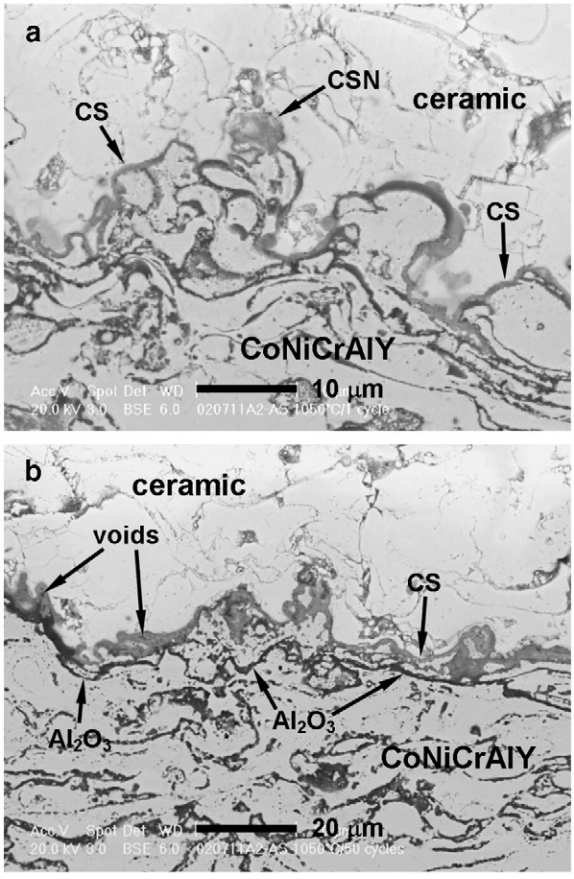

Fig. 3. A TGO layer of predominantly CS formed in as-sprayed CoNiCrAlY after one thermal cycle at 1050 °C (a). A continuous Al_2O_3 layer developed underneath the TGO after 50 thermal cycles (b).

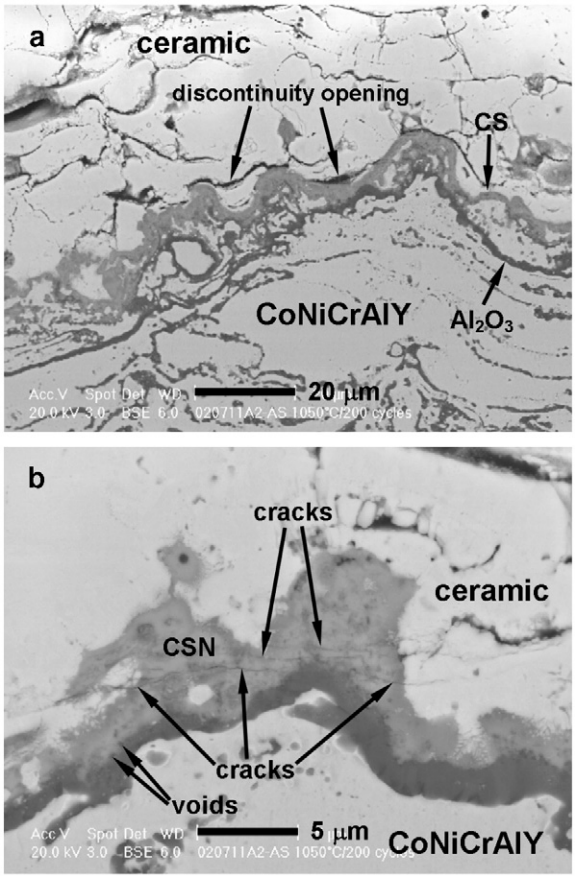

Fig. 4. Discontinuity opening in the ceramic (a) and increased crack nucleation and growth associated with CSN (b) after 200 cycles.

After the VHT, although the Al_2O_3 layer remained discontinuous at the ceramic/bond coat interface, the amount of Al_2O_3 increased (Fig. 2b), compared to that in the as-sprayed condition. A rather uniform and nearly continuous Al_2O_3 layer at the ceramic/bond coat interface developed after the LPOT (Fig. 2c), and a small amount of Al_2O_3·(Co,Ni)$(Cr,Al)_2O_4$·NiO (ASN) also formed within the ceramic/bond coat interface region. After the heat treatments, the aluminum concentration became rather uniform and was <11 at.% in the bond coats of different conditions, lower than that of the feedstock powder

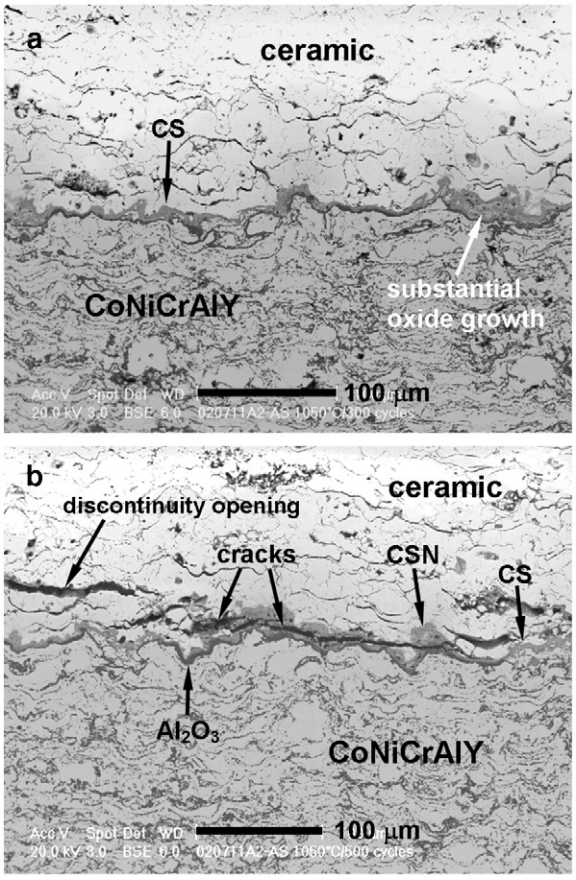

Fig. 5. (a) Substantial oxide growth, indicated by arrow, occurred heterogeneously underneath the CS layer after 300 thermal cycles, and (b) crack propagation within the ceramic topcoat as a result of discontinuity opening and associated with the CSN after 500 cycles.

where the Al level was about 16 at.%. Therefore, to a certain degree the heat treatments can homogenize the highly non-uniform microstructures resulting from thermal spraying of CoNiCrAlY powders in air.

3.2. Cyclic oxidation of as-sprayed TBC

Upon thermal exposure in air, an oxide layer of predominantly $(Cr,Al)_2O_3+(Co,Ni)(Cr,Al)_2O_4$ (CS) formed along the interface between the ceramic topcoat and the bond coat (Fig. 3a). The mixed oxide scale was found to consist of 5–16 at.% Ni+Co and 28–43 at.% Al+Cr. The Al_2O_3 portion in this oxide layer was less than 20%. At the same time, mixed oxide clusters of chromia, spinel and nickel oxide, abbreviated as CSN, also formed at the ceramic/bond coat interface. As such, the TGO formed in the as-sprayed TBC was composed of a CS layer and a number of CSN clusters. As thermal cycling continued, the TGO layer grew thicker (Fig. 3b), and void formation occurred within the TGO (Fig. 3b). In the meantime, crack nucleation appeared to be associated with CSN and CS formation. Moreover, a layer of Al_2O_3 started to form underneath the CS layer (Fig. 3b).

With a further increase of thermal cycles, pre-existing crack-like discontinuities in the ceramic developed into fully open cracks (Fig. 4a) and at the same time, crack nucleation and growth associated with CSN increased (Fig. 4b). Cracks formed between the TGO and the unoxidized bond coat could also be seen. Heterogeneous and substantial growth of mixed oxides, mostly $(Cr,Al)_2O_3$, $(Co,Ni)(Cr,Al)_2O_4$ and NiO, was observed underneath the previously formed CS layer after 300 cycles (Fig. 5a), and moreover, extensive crack propagation associated with the CSN was also observed after 500 cycles (Fig. 5b). The as-sprayed TBC samples failed at around 500 thermal cycles.

3.3. Cyclic oxidation of VHT and LPOT TBCs

The TGO formed in the VHT TBC was composed of a layer of Al_2O_3 and $(Cr,Al)_2O_3+(Co,Ni)(Cr,Al)_2O_4$, as well as some ASN and CSN clusters (Fig. 6a). The Al_2O_3 portion in this TGO was >70%. After 50 thermal cycles, some chromium-rich oxide, with Cr+Al >35 at.% and Ni+Co <7 at.%, started to form underneath the previously formed Al_2O_3 scale (Fig. 6b), which grew into Al_2O_3 during subsequent thermal exposure (Fig. 7a), leading to the complete transformation from Al_2O_3 to CS (Fig. 7b). The formation of chromium-rich oxide underneath the Al_2O_3 layer in plasma-sprayed TBC systems has been reported in previous studies [13,18]. As demonstrated in the as-sprayed TBC, the opening of pre-existing discontinuities also occurred in the VHT samples (Fig. 7a), which led to crack propagation and coalescence, forming longer cracks in the ceramic after

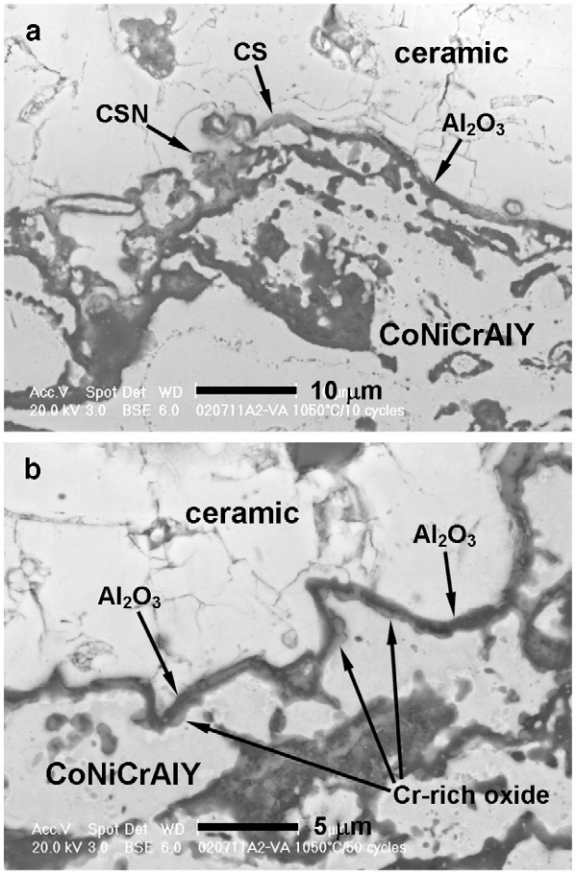

Fig. 6. (a) TGO of >70% Al_2O_3 formed in VHT TBC after 10 cycles, and (b) chromium-rich oxide started to form underneath the previously formed Al_2O_3 scale after 50 cycles.

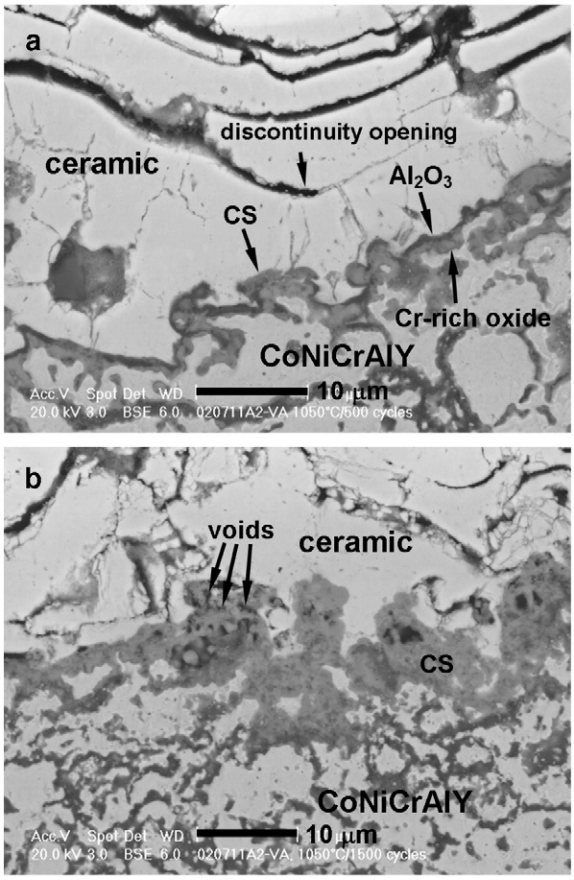

Fig. 7. Micrographs showing (a) the growth of the chromium-rich oxide into previously formed Al_2O_3 scale and discontinuity opening in the ceramic after 500 cycles, and (b) the Al_2O_3 completely transformed to CS after 1500 cycles.

extensive thermal cycling (Fig. 8a). One of the VHT samples lasted only 1470 cycles, but another did not fail until after 2100 cycles, where heterogeneous oxide growth occurred (Fig. 8b).

The TGO formed in the LPOT samples, on the other hand, consisted of more than 90% Al_2O_3 with some minor phase particles present (Fig. 9a), along with a small amount of CS, ASN and CSN clusters. Similar to that in the VHT TBC, chromium-rich oxide started to form at the Al_2O_3/bond coat interface after 50 cycles (Fig. 9b), and grew along the interface during subsequent thermal exposure (Fig. 10). The void formation in the Al_2O_3 scale occurred mostly at the grain boundaries, but the amount was much less than that in the CS layer formed in the as-sprayed TBC. Heterogeneous TGO growth could be observed after 1000 cycles (Fig. 11).

Similar to the as-sprayed and VHT conditions, opening of the pre-existing discontinuities in the ceramic also occurred after a number of thermal cycles, resulting in formation of cracks (Fig. 10b). Much longer cracks were seen in the ceramic near the TGO, some of which appeared at a distance of ~150 μm above the TGO layer after extensive thermal cycling (Fig. 11a). The microcracks formed at the TGO/bond coat interface (Fig. 10) seem to have little contribution to the dominant crack propagation in the TBC. The LPOT samples failed after 1670 and 1830 cycles.

3.4. TGO growth and crack propagation in the TBCs

Since the TGO formed on a rough interface, sectioning of the TBC samples could not always reveal the true thickness of the TGO. In addition, it was noticeable that the TGO grew heterogeneously along the ceramic/bond coat interface, especially when CSN clusters were formed between the ceramic topcoat and the bond coat (Figs. 5, 8 and 11). To take into account the entire TGO, an equivalent TGO thickness, δ_{eq}, is defined as:

$$\delta_{eq} = \frac{\sum(\text{cross sectional TGO area})}{\sum(\text{cross sectional length of TC/BC interface})} \quad (1)$$

The relationship between δ_{eq}^2 and number of thermal cycles (Fig. 12) shows a parabolic growth of TGO, which is consistent with previous observations [10–17]; however, an acceleration of TGO thickening is noticeable. A similar observation was made in a FeCrAl alloy by determining the weight change under oxidation conditions [19]. This clearly shows that the growth of TGOs exhibits a three-stage growth behaviour: i) an instantaneous TGO growth at the onset of oxidation, ii) a steady-state growth and iii) an acceleration stage, which somewhat resembles the primary, secondary and tertiary stages of creep, respectively. It also shows that the growth of TGOs in the VHT and LPOT

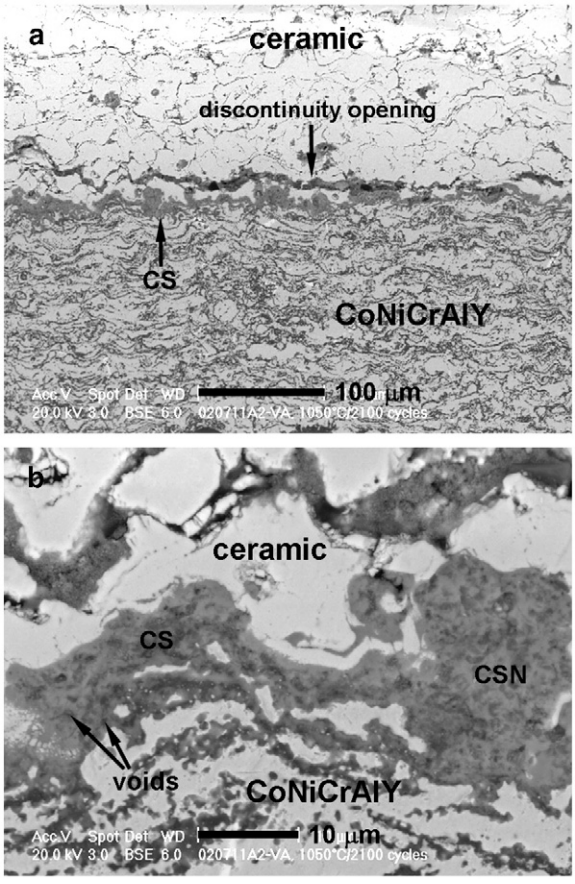

Fig. 8. (a) Large crack formed within the ceramic/bond coat interface region as a result of discontinuity opening and growth, along with crack nucleation and propagation associated with TGO development, and (b) a close-up view of (a) showing heterogeneous and substantial TGO growth after 2100 cycles.

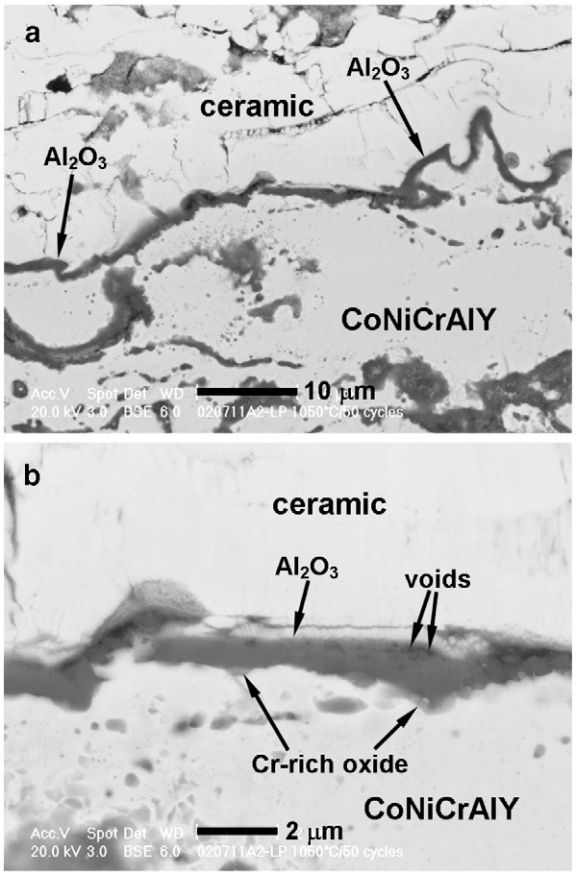

Fig. 9. (a) TGO layer with >90% Al_2O_3 between the ceramic and the bond coat in LPOT TBC after 50 cycles, and (b) an enlarged area of (a) showing Cr-rich oxide formed between the Al_2O_3 layer and bond coat.

TBCs has an extended steady-state growth region, compared to the as-sprayed TBC. The VHT and LPOT TBCs have a comparable TGO growth rate in the beginning; however, the LPOT TBC exhibits an earlier onset of the tertiary growth stage.

Fig. 13 shows the maximum crack length in the TBCs at the predetermined thermal cycle intervals, indicating that cracks propagate also much faster in the as-sprayed TBC than in the VHT and LPOT TBCs. When plotting the maximum crack length as a function of TGO thickness, as shown in Fig. 14, it appears that crack length increases with TGO thickness, even though the microstructure of the TGOs varies. Regression analysis shows that the relationship between the maximum crack length in the TBC and TGO thickness can be expressed by a power law (Fig. 14), i.e. $a_{max}=k\delta_{eq}^{n}$, where k and n are constants. The value of n is determined to be 0.597.

4. Discussion

4.1. Oxide formation

It was believed that Al_2O_3 would form first in the CoNiCrAlY bond coats (Fig. 15) during thermal exposure in air [20]. However, the present study shows that in the as-sprayed TBC the TGO consisted of a chromia+spinel layer and mixed oxide clusters, other than the Al_2O_3. The formation of $Ni(Cr,Al)_2O_4$ and NiO has been reported by many researchers [1–6], which was attributed to the compositional inhomogeneity in the thermally sprayed TBC systems. The APS-CoNiCrAlY bond coat had a lower aluminum concentration than the CoNiCrAlY powder, due to the partial oxidation during the APS deposition process. Lower aluminum concentration in as-sprayed samples leads to movement from the Al_2O_3 region into the $(Cr,Al)_2O_3$ region and then eventually to the NiO region (Fig. 15).

The VHT and LPOT, on the other hand, imposed a low oxygen pressure environment that promotes the formation of Al_2O_3, because of the reduced oxygen activity in the gas phase, since $NiAl_2O_4$ and NiO will form at a higher oxygen activity compared to Al_2O_3. It was suggested that the formation of $NiAl_2O_4$ and NiO could be avoided in the Ni–Al system at 940 °C with an oxygen pressure $<4.9\times10^{-14}$ atm ($P_{O_2}<5\times10^{-9}$ Pa) [21]. This study also shows that $NiAl_2O_4$ and NiO formation can be suppressed noticeably in the CoNiCrAlY at a much higher oxygen pressure ($P_{O_2}\approx0.056$ Pa). Nevertheless, in the VHT, the oxygen pressure is too low ($P_{O_2}<2.8\times10^{-4}$ Pa) to develop a continuous Al_2O_3 layer at 1080 °C (Fig. 2). Therefore, a heat treatment in a low oxygen pressure environment of $P_{O_2}=0.01$–0.1 Pa may promote the formation of a nearly continuous thin Al_2O_3 layer. The formation of other minor oxide particles, such as (Co,Ni)$(Cr,Al)_2O_4$/$(Cr,Al)_2O_3$ and (Co,Ni)O, could be caused by local shortage of the aluminum content in the nearby bond coat.

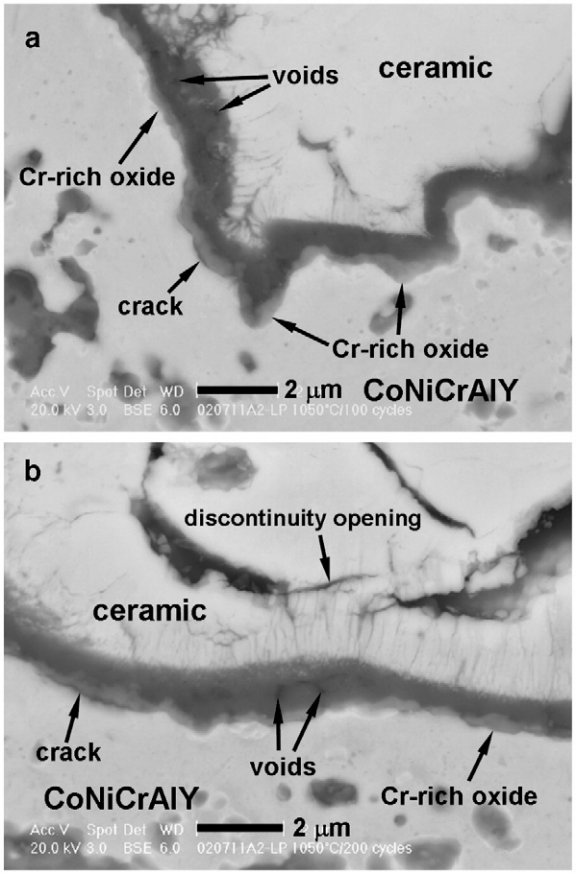

Fig. 10. Void formation within the Al_2O_3 layer and interfacial cracks at the TGO/bond coat interface in LPOT TBC, after (a) 100 cycles and (b) 200 cycles.

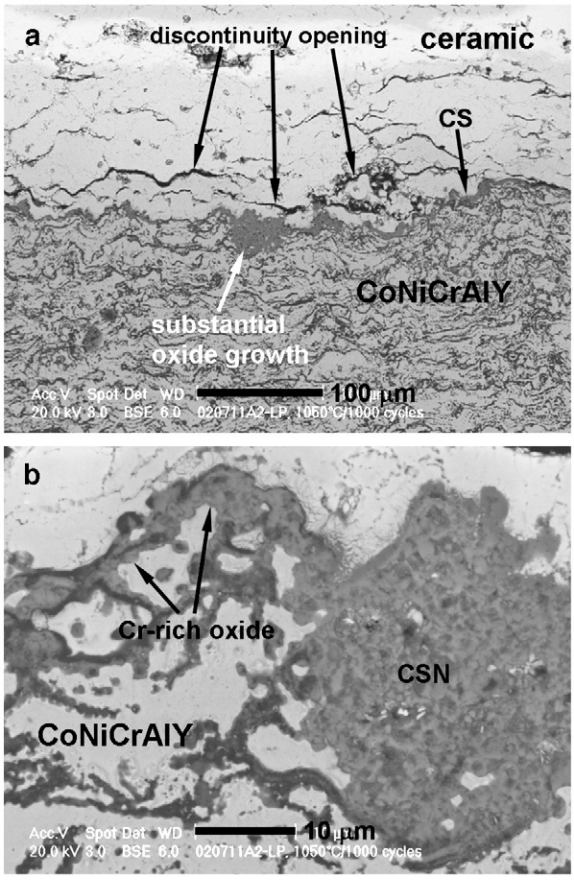

Fig. 11. (a) Cracks in the ceramic topcoat as a result of discontinuity opening and heterogeneous TGO growth in the LPOT TBC after 1000 cycles, and (b) a close-up look of (a) showing chromium-rich oxide growing into previously formed Al_2O_3 scale.

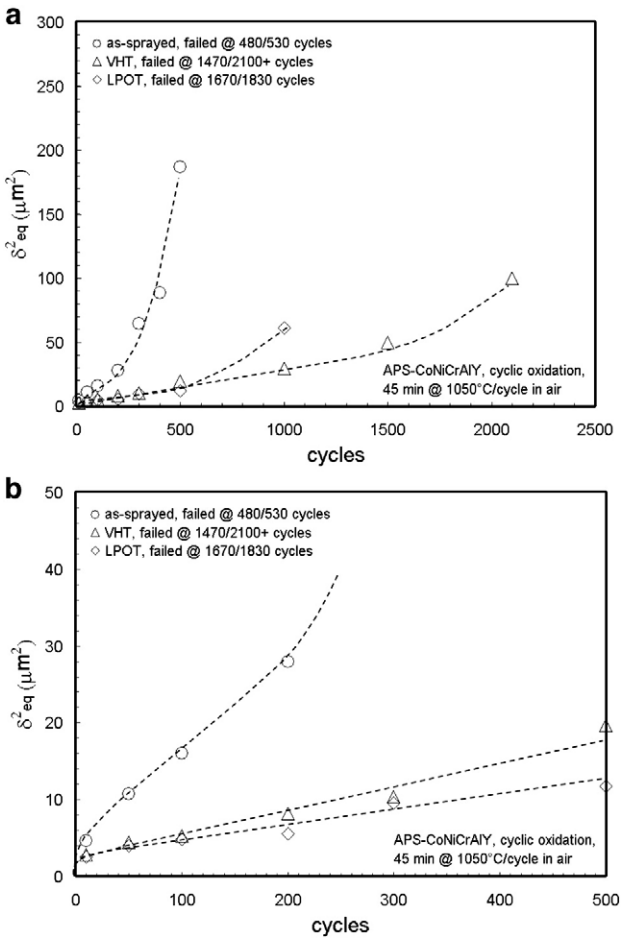

Fig. 12. (a) The growth of TGOs in APS-TBC during cyclic oxidation, and (b) the early stage of oxidation.

When a continuous oxide layer formed at the ceramic/bond coat interface, the oxygen partial pressure at the oxide/metal interface would decrease to the formation pressure of Al_2O_3, which is the lowest value among the various species present [22], making Al_2O_3 the most favorable oxide product. However, as a result of aluminum depletion in the bond coat such that a composition was reached at which other oxide(s) could form [23], chromium-rich oxide started to form at the Al_2O_3/bond coat interface after a number of thermal cycles (Figs. 6b, 9b and 10). The transformation of the initially formed Al_2O_3 layer into a chromia+spinel layer in the VHT and LPOT samples (Figs. 7 and 11) can probably be attributed to the reaction of Al_2O_3 with Cr and/or Ni [18,23] from the chromium-rich oxide layer underneath and/or the unoxidized bond coat. As thermal exposure proceeds, transient oxidation will occur and consequently, the formation and growth of spinel and nickel oxide will dominate the afterward TGO thickening.

4.2. TGO growth

It is noticeable that TGO growth exhibits a three-stage growth behaviour (Fig. 12), which is consistent with previous observation in an FeCrAl alloy [19]. The growth of TGO started to accelerate at ~300 cycles in the as-sprayed TBC, at ~2000 cycles in the VHT TBC and ~1000 cycles in the LPOT TBC. The onset of this tertiary stage was clearly associated with heterogeneous oxidation (Figs. 5a, 8 and 11). In the as-sprayed TBC, this heterogeneous oxidation occurred underneath the previously formed CS layer, but in the VHT and LPOT TBCs, it occurred by transformation

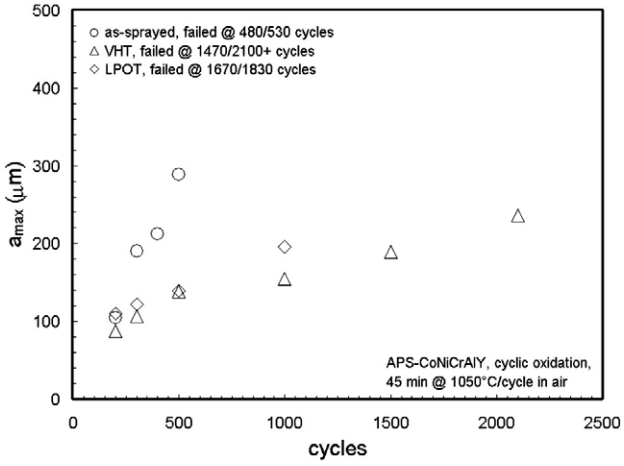

Fig. 13. The maximum crack length in the TBC as a function of the number of thermal cycles.

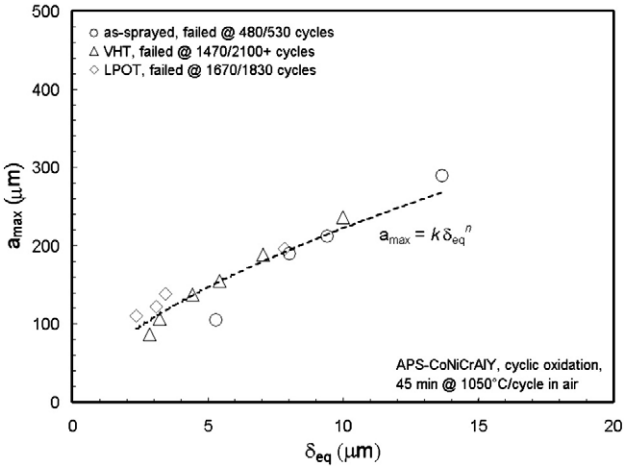

Fig. 14. The maximum crack length in the TBC as a function of equivalent TGO thickness.

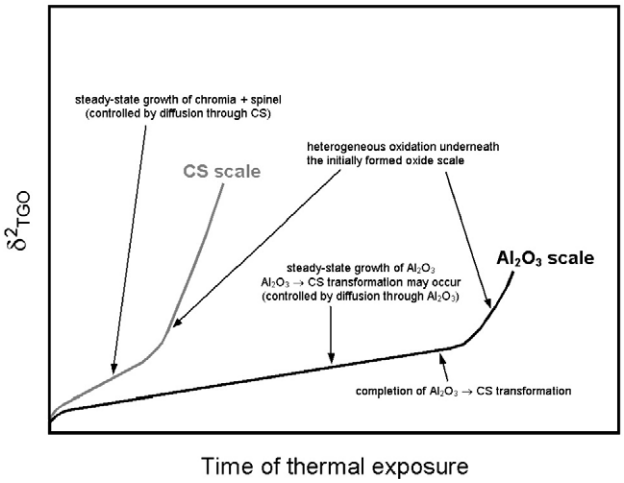

Fig. 16. A systematic description of TGO thickening process.

from the Al_2O_3 layer to chromia + spinel and subsequent heterogeneous oxidation underneath, after extensive thermal exposure.

The growth of TGOs in the VHT and LPOT TBCs shows an extended steady-state stage, compared to that in the as-sprayed TBC. The higher TGO growth rate in the as-sprayed TBC can be attributed to the CS layer formed at the ceramic/bond coat interface, since diffusion through chromia is faster than through Al_2O_3 [24,25]. As aluminum further depletes from the bond coat, heterogeneous oxidation will occur underneath the TGO, leading to the onset of accelerated TGO growth (Fig. 16). On the other hand, TGO growth in the VHT and LPOT TBCs would remain slow due to the slow diffusion through the Al_2O_3 before the initially formed Al_2O_3 completely transformed to chromia + spinel, which prolonged the steady-state TGO growth. As aluminum was further depleted in the bond coat, the initially formed Al_2O_3 layer would completely transform into a CS layer at the ceramic/bond coat interface, and consequently, heterogeneous oxidation underneath the TGO would occur, leading to an accelerated TGO growth.

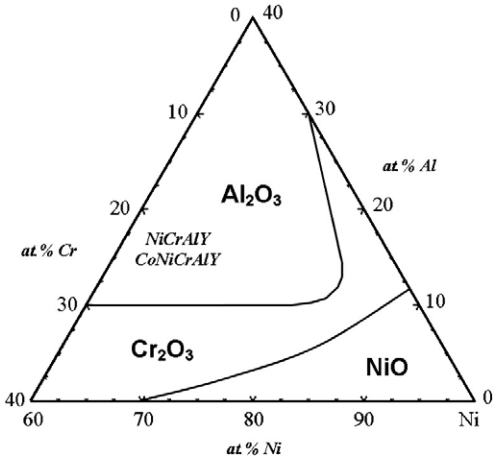

Fig. 15. Type of oxide scale formed in Ni–Cr–Al system upon thermal exposure in air, after Hindam and Whittle [20]. The Amdry 9951 CoNiCrAlY powder contains ~16 at.% Al and ~21 at.% Cr.

Fig. 12 also shows a difference in the lengths of steady-state TGO growth stages in the VHT and LPOT samples. Since the lifetime of the VHT TBC spans from 1470 to 2100+ cycles, and that of the LPOT ones falls in between, it is suspected that such a difference might be a result of non-uniform microstructure/composition of the thermally sprayed coating system. Considering that the VHT can only develop a discontinuous Al_2O_3 layer at the ceramic/bond coat interface, whereas the LPOT produces a nearly continuous Al_2O_3 layer, it can be expected that the latter will enable the APS-TBC to have a rather uniform performance. Moreover, it seems that the LPOT could be further optimized by shortening the heat treatment time at 1080 °C, to produce a nearly continuous but thinner Al_2O_3 layer at the ceramic/bond coat interface.

4.3. Crack nucleation and growth

Crack propagation in the TBCs during thermal cycling appears to proceed via discontinuity opening and growth in the ceramic (Figs. 4a, 7a and 10b), which is assisted by crack nucleation and propagation associated with the TGO (Figs. 5b, 8a and 11a). It can be seen that CSN clusters and the CS layer are more susceptible to crack nucleation and propagation (Fig. 4b). Since the cracking behaviour was examined through random sectioning, some of the discontinuity opening could also result from cracking associated with CSN and CS near the cross-sectioned surface. On the other hand, VHT and LPOT promote the formation of an Al_2O_3 layer at the ceramic/bond coat interface that, albeit not continuous, is more cracking resistant at the early stage of thermal cycling. As thermal exposure further proceeds, the initially formed Al_2O_3 transforms to chromia + spinel, resulting in increased cracking associated with the TGO and consequently, longer cracks within the ceramic/bond coat interface region (Fig. 8a).

The maximum crack length (a_{max}) in the TBC and the TGO thickness (δ_{eq}) exhibit a power law relationship

$$a_{max} = k\delta_{eq}^{n} \quad (2)$$

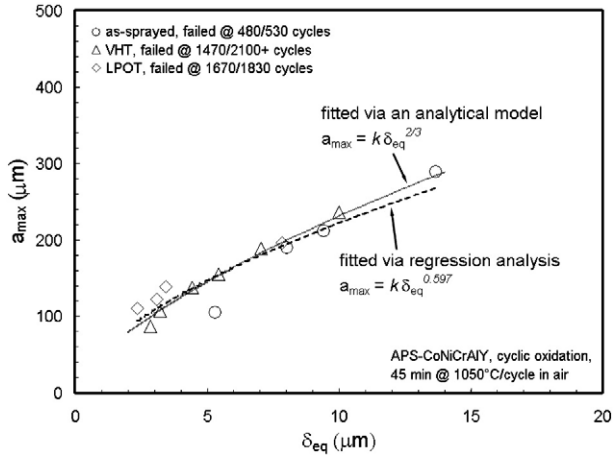

Fig. 17. Correlation between maximum crack length and equivalent TGO thickness determined by a regression analysis and based on an analytical model.

where k and n are constants. Regression analysis shows that $n=0.597$. An analytical model proposed by Evans and co-workers [26] has shown that TGO thickness in a TBC can be expressed as

$$h = \frac{2\sqrt{\pi}(1-\nu^2)\,mK}{(m-1)RE}\,a^{3/2} \tag{3}$$

h	TGO thickness
a	half crack length
R	radius of the imperfection
m	ratio of volume change
E	Young's modulus of the TBC
ν	Poisson's ratio
K	stress intensity factor

Considering crack propagation during thermal cycling proceeds via discontinuity opening and coalescence in the ceramic as well as crack nucleation and propagation associated with the TGO, $2R$ could be taken as the diameter of an individual splat, whereas $2a$ might be considered as the distance between two neighboring discontinuities. For crack propagation in a brittle material, when K is equal to K_{IC} (the fracture toughness), crack length and TGO thickness would therefore show the following relationship:

$$a = kh^{2/3} \tag{4}$$

where k is a constant. The theoretical exponent derived by Evans and co-workers is 0.667, which is close to the experimental value of 0.597 determined in this study. Therefore, it is likely that such a power law relationship between the maximum crack length and the TGO thickness does exist in the APS-TBC. Fig. 17 shows a close match between the results determined by the regression analysis and based on Evans' model.

The as-sprayed TBC failed at 480/530 cycles, as shown in Fig. 13, from which it can be estimated that the critical crack length in the TBC is ~300 μm, which corresponds to a critical TGO thickness of about 15 μm (Fig. 14). As such, the VHT samples can be expected to have a lifetime of about 2500 cycles, while the LPOT samples may last 1500–2000 cycles, based on the determined TGO growth curves (Fig. 12).

It has been shown that the critical crack size for initiating TBC spallation is somehow related to the topcoat thickness [27]. Therefore, determination of the relationship between crack length and TGO thickness may be helpful in TBC life prediction. This suggests that the nature of such a relationship merits further investigation in both numerical and experimental studies.

5. Conclusions

The present work investigated the influence of pre-oxidation treatments in low-pressure oxygen environments on the cyclic oxidation behaviour of an air-plasma-sprayed Co–32Ni–21Cr–8Al–0.5Y (wt.%) bond coat. The major findings on the cyclic oxidation behaviour in relation to TGO growth and crack nucleation and growth can be summarized as follows:

(1) Both VHT and LPOT can suppress the formation of detrimental mixed oxides, and develop a TGO comprised of a predominantly Al_2O_3 layer; however, this Al_2O_3 layer is not stable as a result of aluminum depletion in the bond coat after extensive thermal exposure;
(2) The development of TGOs exhibits a three-stage growth phenomenon, i.e., i) an instantaneous TGO growth stage at the onset of oxidation, ii) a steady-state growth stage and iii) an accelerated growth stage. The VHT and LPOT not only decrease the growth rate of the TGO, but also extend the steady-state growth stage;
(3) Crack propagation in the APS-TBC during thermal cycling proceeds via discontinuity opening and growth in the ceramic, and is assisted by crack nucleation and propagation associated with the TGO; both VHT and LPOT decrease the crack growth rate via reducing the detrimental oxide formation during thermal exposure, leading to an improved durability;
(4) A power law relationship between the maximum crack length in the TBC and TGO thickness likely exists, which may be useful to the life prediction for the thermally sprayed TBCs.

Acknowledgements

The authors thank Sylvain Bélanger of the Industrial Materials Institute of NRC Canada for thermal spraying the TBC samples, and Peter L'Abbe of the Institute for Chemical Process and Environmental Technology of NRC Canada for preparing the samples for LPOT. They are also grateful to Robert McKellar and Ryan MacNeil of NRC-IAR-SMPL for their help in VHT and oxidation testing. The support from the SURFTEC consortium is also appreciated.

References

[1] J.A. Haynes, E.D. Rigney, M.K. Ferber, W.D. Porter, Surf. Coat. Technol. 86-87 (1996) 102.
[2] E.A.G. Shillington, D.R. Clarke, Acta Mater. 47 (1999) 1297.
[3] A. Rabiei, A.G. Evans, Acta Mater. 48 (2000) 3963.
[4] C.H. Lee, H.K. Kim, H.S. Choi, H.S. Ahn, Surf. Coat. Technol. 124 (2000) 1.

[5] L. Ajdelsztajn, J.A. Picas, G.E. Kim, F.L. Bastian, J. Schoenung, V. Provenzano, Mater. Sci. Eng. A338 (2002) 33.
[6] W.R. Chen, X. Wu, P.C. Patnaik, J.-P. Immarigeon, Proceedings from the 1st International Surface Engineering Congress and the 13th IFHTSE Congress, Columbus, Ohio, 2002, p. 535.
[7] R.A. Miller, C.E. Lowell, Thin Solid Films 95 (1982) 265.
[8] D. Monceau, F. Crabos, A. Malié, B. Pieraggi, Mat. Sci. Forum 369-372 (2001) 607.
[9] S. Takahashi, M. Yoshiba, Y. Harada, Mat. Sci. Forum 461-464 (2004) 367.
[10] M.A. Gedwill, "Improved Bond Coat Coatings for Use with Thermal Barrier Coatings", NASA TM-81567, 1980.
[11] R.A. Miller, The 112th annual meeting of The Metallurgical Society AIME, Atlanta, GA, 1982, p. 293.
[12] W. Brandl, H.J. Grabke, D. Toma, J. Krüger, Surf. Coat. Technol. 86-87 (1996) 41.
[13] J.A. Haynes, M.K. Ferber, W.D. Porter, E.D. Rigney, Oxid. Met. 52 (1999) 31.
[14] K.S. Chan, N.S. Cheruvu, GT2004-53383, Proceedings of ASME Turbo Expo 2004, Power for Land, Sea, and Air, Vienna, Austria, 2004.
[15] S.M. Meier, D.M. Nissley, K.D. Sheffler, ASME 91-GT-40, International Gas Turbine and Aeroengine Congress and Exposition, Orlando, FL, 1991.
[16] Kh.G. Schmitt-Thomas, M. Hertter, Surf. Coat. Technol. 120-121 (1999) 84.
[17] W.R. Chen, X. Wu, B.R. Marple, P.C. Patnaik, Surf. Coat. Technol. 197 (2005) 109.
[18] P. Niranatlumpong, C.B. Ponton, H.E. Evans, Oxid. Met. 53 (2000) 241.
[19] G.H. Meier, F.S. Pettit, J.L. Smialek, Mater. Corros. 46 (1995) 232.
[20] H. Hindam, D.P. Whittle, Oxid. Met. 18 (1982) 245.
[21] V. Kuznetsov, in: G. Petzow, G. Effenberg (Eds.), Ternary Alloys, vol. 7, VCH Publishers, New York, NY, 1993, p. 434.
[22] M.W. Brumm, H.J. Grabke, Corros. Sci. 33 (1992) 1677.
[23] F.S. Pettit, Trans. Metall. Soc. AIME 239 (1967) 1296.
[24] G.R. Wallwork, A.Z. Hed, Oxid. Met. 3 (1971) 171.
[25] F.S. Pettit, G.H. Meier, in: M. Gell, C.S. Kartovich, R.H. Bricknel, W.B. Kent, J.F. Radovich (Eds.), Superalloys, The Metal Society AIME, Warrendale, PA, 1984, p. 651.
[26] A.G. Evans, M.Y. He, J.W. Hutchinson, Prog. Mater. Sci. 46 (2001) 249.
[27] D. Zhu, S.R. Choi, R.A. Miller, Surf. Coat. Technol. 188-189 (2004) 146.